

## NUMERICAL INVESTIGATION OF CLOSURES FOR INTERFACE FORCES IN DISPERSED FLOWS USING A 3D FRONT TRACKING MODEL

Wouter Dijkhuizen, Martin van Sint Annaland<sup>1</sup> and Hans Kuipers.

Chemical Reaction Engineering group, University of Twente, The Netherlands.

<sup>1</sup> Corresponding author. Tel. +31-53-4894478; fax +31-53-4892882.

E-mail address: M.vanSintAnnaland@utwente.nl

### ABSTRACT

Closures for the drag, virtual mass and lift forces acting on a single air bubble or toluene droplet in water have been studied using a 3D Front Tracking model. The numerical implementation of the FT model was improved to allow simulations of very small air bubbles rising in water (~1 mm) using realistic physical properties. For this system the surface tension force, density ratio and the Reynolds number all are very high. The computed drag force coefficient for air bubbles in water (1-5 mm diameter) compare reasonably well with experimental data obtained results using ultra pure water. Similar drag coefficients were computed for toluene droplets rising in water, as expected since these two systems possess comparable Morton numbers. For the virtual mass coefficient a value of 0.53 was found on a 80x80x80 grid for air bubbles in water, which compares very well with the theoretical value of 0.50. Finally, the lift force coefficient was computed for a 4 mm air bubble rising in water. A value of 0.5 was computed, which is slightly higher than reported experimentally at somewhat lower Reynolds numbers.

### NOMENCLATURE

$C_D$	drag force coefficient	[-]
$C_L$	lift force coefficient	[-]
$C_{VM}$	virtual mass coefficient	[-]
$D$	distribution function	[-]
$F$	phase fraction	[-]
$F_\sigma$	surface tension force density	[N·m <sup>-3</sup> ]
$\mathbf{G}$	phase fraction gradient	[-]
$\mathbf{g}$	gravity constant	[m·s <sup>-2</sup> ]
$M$	Morton number	[-]
$\mathbf{n}$	normal vector	[-]
$p$	pressure	[N·m <sup>-2</sup> ]
$Re$	Reynolds number	[-]
$s$	surface	[m <sup>2</sup> ]
$t$	time	[s]
$\mathbf{t}_m$	tangential unit vector	[-]
$\mathbf{t}_{m,l}$	tangential vector along edge l	[m]
$\mathbf{u}$	velocity	[m·s <sup>-1</sup> ]
$\mathbf{u}_l$	liquid velocity	[m·s <sup>-1</sup> ]
$\mathbf{w}_b$	bubble velocity	[m·s <sup>-1</sup> ]
$\rho$	density	[kg·m <sup>-3</sup> ]
$\mu$	dynamic viscosity	[kg·m <sup>-1</sup> ·s <sup>-1</sup> ]
$\sigma$	surface tension	[N·m <sup>-1</sup> ]
$\Delta x, \Delta y, \Delta z$	grid dimensions	[m]

### INTRODUCTION

Multiphase gas/liquid and gas/liquid/liquid flows are widely encountered, in natural phenomena as well as in industry. For instance, the oil industry has to deal with complex flows consisting of oil droplets and gas bubbles dispersed in water. More examples include Fischer-Tropsch and other important chemical processes. Because of the wide range of length and time scales, it is virtually impossible to capture all the details of the flow field with currently available computational resources. Therefore a successful description of multi-phase flows therefore has to be based on a sound multi-level modelling approach (van Sint Annaland et al., 2003):

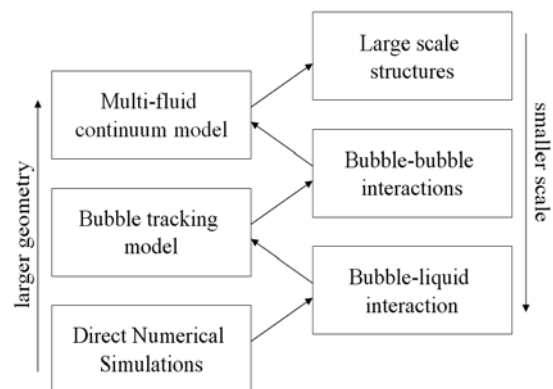


**Figure 1:** Multi-level modelling approach for multi-phase dispersed gas-liquid flow. The exchange of information is indicated by arrows.

At the smallest time and length scale a Direct Numerical Simulation (DNS) is used to study the behaviour of a single or a few gas bubbles or liquid droplets. These simulations backed up by dedicated detailed experiments can be used to derive closures for the bubble-liquid interaction, which can then be used in higher level models. One step up, the Euler-Lagrange model can be used to study the interactions between a large number of bubbles and the influence of these interactions on the macroscopic flow structure. In this model each bubble is represented in a discrete fashion and the forces on each bubble are computed from closure equations. In this approach a large number of bubbles (~100,000) can be simulated with acceptable computation time. However, in industrial applications multi-phase flows with even a much higher

number of dispersed elements are encountered, which requires a continuum approach. At this highest level of modelling the Euler-Euler or multi-fluid continuum models, bubbles lose their discrete identity, which enables the simulation of very large systems and study large-scale heterogeneous structures in the flow.

It has proven to be a daunting task to accurately describe the behaviour of gas-liquid or liquid-liquid systems with the higher level models, because detailed knowledge on the behaviour of single bubbles or droplets in complex flow fields is lacking. For example, even the behaviour of a single air bubble rising in quiescent water is not yet completely understood: not only physical properties like the density, viscosity and surface tension affect the behaviour of the bubbles, but also small amounts of surface active impurities (Grace et al., 1976). More recently, Wu and Gharib (2002) and Tomiyama et al. (2002a) independently pointed out that the initial shape of the bubble can affect its terminal rise velocity. This illustrates the intrinsic complexities in performing dedicated experiments.

The problem in the description of the motion of a single bubble or droplet arises from the complex interaction between the bubble shape dynamics and the flow field in its vicinity. This is particularly difficult at high Reynolds numbers, which are encountered in the industrially important case of dispersed elements in water. With the advances that have been made in CFD during the last decades, now the shape and interface dynamics can be studied in great detail. In this study a DNS has been used to study the behaviour of air bubbles and toluene droplets rising in water.

When it comes to DNS several models have been proposed and used in the literature, where it is important to realise that every model has its own strong and weak points (van Sint Annaland et al., 2005a). By far the most popular model is the Volume Of Fluid (VOF) model, which typically involves reconstruction of the interface using the spatial distribution of the volume fraction of the phases. The major advantage of this model is that it is relatively easy to implement and the volume of the dispersed elements is very well conserved. However these advantages come at a high cost: the interface is not explicitly tracked, but has to be reconstructed from the phase fractions. First of all this causes problems when calculating the surface tension force, which is a singular force acting on the interface. Secondly a poor interface reconstruction combined with a large density ratio may cause the numerical method to become unstable. Also parasitic currents in the vicinity of the interface may develop. These drawbacks of the VOF method are especially limiting for small air bubbles ( $\sim 1$  mm) in water, where a high density ratio and a high surface tension force are combined.

In this work a full 3D Front Tracking (FT) model is used, based on the work of Unverdi and Tryggvason (1992). The advantage of this model is that the interface is explicitly tracked by interconnected points which form triangular markers. In sharp contrast with VOF this makes it possible to describe the shape and location of the interface with a very high accuracy. The first benefit is that the accuracy of the surface tension force calculation

can be improved (Popinet and Zaleski, 1998). Secondly because there is no interface reconstruction, parasitic currents are greatly reduced. However, this comes at a price: the volume of the dispersed phases is not intrinsically conserved and because of deformation, marker points have to be periodically added and removed (surface remeshing). For a detailed comparison of different DNS methods the interested reader is referred to Scardovelli and Zaleski (1999).

3D Front Tracking was used in this work to calculate the drag, virtual mass and lift forces directly, without the need for any kind of closures. The results of the numerical simulations are compared with experimental data. In all of our simulations realistic physical properties were used, for instance a density ratio of 800 for air bubbles in water. Before this was possible, some modifications had to be made to the original model, in order to improve mass conservation for small air bubbles in water. These modifications were extensively verified using standard test cases as reported by van Sint Annaland et al. (2005b).

## FRONT TRACKING MODEL

### Governing equations

In the FT model the Navier-Stokes equations are solved together with the continuity equation for incompressible media:

$$\nabla \cdot \mathbf{u} = 0 \quad (1)$$

$$\frac{\partial}{\partial t}(\rho \mathbf{u}) + \nabla \cdot \rho \mathbf{u} \mathbf{u} = -\nabla p + \rho \mathbf{g} + \nabla \cdot \mu \left[ (\nabla \mathbf{u}) + (\nabla \mathbf{u})^T \right] + \mathbf{F}_\sigma \quad (2)$$

where the density  $\rho$  and the viscosity  $\mu$  are locally averaged over all the phases present, based on the phase fraction  $F_i$ . The surface tension force is included as a volumetric force density  $\mathbf{F}_\sigma$  acting only in the vicinity of the interface.

The Navier Stokes equations are solved on a staggered Cartesian mesh with a finite volume technique using an implicit treatment of the pressure gradient and an explicit treatment of the convection and diffusion terms. For the convection term a second order flux delimited Barton scheme is used (Centrella and Wilson, 1984) and for the diffusion term a standard second order finite difference scheme is used. To be able to simulate large density ratios, the Navier-Stokes equations are rewritten in their non-conservative form using the continuity equation (Van Sint Annaland et al., 2003):

$$\rho \left[ \frac{\partial \mathbf{u}}{\partial t} + \nabla \cdot \mathbf{u} \mathbf{u} \right] = -\nabla p + \rho \mathbf{g} + \nabla \cdot \mu \left[ (\nabla \mathbf{u}) + (\nabla \mathbf{u})^T \right] + \mathbf{F}_\sigma \quad (3)$$

A two step projection-correction method is used to solve the two equations: first the velocity is calculated using all the explicit terms in the Navier-Stokes equations and secondly a robust ICCG method is used to calculate the pressure correction to satisfy the incompressibility

constraint. A higher order discretisation scheme was applied for the divergence operator.

### Average fluid properties

For the local density linear weighing of all the phase fractions is used:

$$\rho = \sum_{i=1}^{nphases} F_i \rho_i \quad (4)$$

where  $F_i$  represents the fraction of phase  $i$ . Usually the viscosity is also linearly averaged, but here a more fundamental approach is used based on harmonic averaging of the kinematic viscosities (Prosperetti, 2001):

$$\frac{\rho}{\mu} = \sum_{i=1}^{nphases} F_i \frac{\rho_i}{\mu_i} \quad (5)$$

### Surface tension

Making direct use of the triangulation of the interface, the surface tension force acting on marker  $m$  is calculated via a contour integral over the tensile forces (see Fig. 2):

$$\mathbf{F}_{\sigma,m} = \frac{\sigma}{\Delta x \Delta y \Delta z} \oint_l (\mathbf{t}_m \times \mathbf{n}_m) dl \quad (6)$$

where  $\mathbf{t}_m$  is the counter clockwise unit tangent vector along the edges of the marker  $m$  and  $l$  is the length of these tangent vectors (the perimeter of the marker).

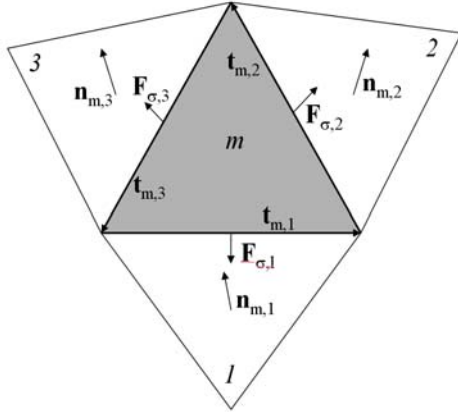


**Figure 2:** Schematic illustration of the direct surface tension force calculation.

This method avoids the computation of the numerically inaccurate curvature and can be used for surfaces with a very high curvature with less numerical instability and better accuracy (Gunsing, 2004). The surface tension force is mapped on to the Eulerian grid using a summation over all the markers  $m$  and their edges  $l$ :

$$\mathbf{F}_\sigma = \frac{\sum_m \sum_l D(\mathbf{x} - \mathbf{x}_{m,l}) \sigma (\mathbf{t}_{m,l} \times \mathbf{n}_{m,l})}{\Delta x \Delta y \Delta z} \quad (7)$$

where  $\mathbf{t}_{m,l}$  is the tangential vector and  $D$  is the distribution kernel, for which in this work density weighing (Deen et

al., 2004) is used. Density weighing avoids mapping the surface tension force to a cell with a low mass, which can cause large distortions of the velocity field near the interface. Tryggvason et al. (2001) use a polynomial fit to obtain the normal and tangential vectors, but with our method the surface tension force is calculated directly from the discrete triangulation.

### Calculation of the phase fractions

In the FT model the phase fractions are calculated by a method proposed by Unverdi and Tryggvason (1992):

$$\begin{aligned} \nabla^2 F &= \nabla \cdot \mathbf{G} \\ \mathbf{G} &= \sum_m D(\mathbf{x} - \mathbf{x}_m) \mathbf{n}_m \Delta s_m \end{aligned} \quad (8)$$

where  $\mathbf{n}_m$  is the outwards pointing normal and  $\Delta s_m$  is the surface of the marker. First the gradient  $\mathbf{G}$  is calculated from the interface markers, after which an ICCG method is used to solve this Poisson equation.

### Updating the interface

Once the flow field has been found on the Eulerian grid, each marker point of the interface triangulation is moved with the local flow field. After some time the surface grid will become deformed. Some markers will become too large or too stretched, while others become too small. To maintain an adequate resolution, points will have to be added at some places and removed at other places. In this work a similar approach as described by Unverdi and Tryggvason (1992) is followed.

### DERIVATION OF INTERFACE FORCES

In order to provide closures for discrete elements models, where the bubbles or droplets are considered to be spherical, the drag, virtual mass and lift coefficients are also derived assuming spherical entities. The effects of the shape of the bubble are thus implicitly lumped in the coefficients.

#### Drag force

Both the drag and virtual mass forces can be obtained from a simulation where initially the fluid is at rest and the bubble or droplet is released as a perfect sphere.

The drag force coefficient  $C_D$  can be computed from the terminal rise velocity of the dispersed element via a simple stationary force balance in the  $z$ -direction:

$$C_D = \frac{4}{3} \frac{(\rho_l - \rho_g) |\mathbf{g}| d_e}{\rho_l |\mathbf{w}_b| w_{b,z}} \quad (9)$$

where  $w_b$  is the bubble rise velocity and  $d_e$  the equivalent sphere diameter.

#### Virtual mass force

Virtual or added mass is the additional mass that has to be accelerated apart from the dispersed element itself, caused by the fact that the surrounding liquid has to be moved

away from the bubble to let it rise. For a perfect sphere the analytical value is  $\frac{1}{2}$  (Lamb, 1932), meaning that the equivalent of half the bubble volume of liquid is added to the mass of the dispersed element when it accelerates.

The virtual mass force coefficient  $C_{VM}$  can be computed from an instationary force balance in the z-direction, yielding the following expression:

$$C_{VM} = -\frac{\rho_g}{\rho_l} + \frac{(\rho_l - \rho_g)|\mathbf{g}|}{\rho_l \frac{dw_{b,z}}{dt}} \quad (10)$$

It can be seen that for low pressure gas bubbles ( $\rho_l \gg \rho_g$ ) the equation reduces to:

$$C_{VM} = \frac{|\mathbf{g}|}{\frac{dw_{b,z}}{dt}} \quad (11)$$

### Lift force

When a linear shear field is applied to a small dispersed element it will move towards the lower velocity, while larger bubbles or droplets will move towards the higher velocity. Tomiyama et al. (2002b) found experimentally for different viscous systems ( $M > 10^{5.5}$ ) that this transition occurs at an Eötvös number of 6.

Finally the lift force coefficient  $C_L$  can be found by combining force balances in the direction of the velocity gradient (x-direction) and the vertical direction.

$$C_L = \frac{\rho_l - \rho_g}{\rho_l} \frac{|\mathbf{g}|(\mathbf{w}_{b,z} - u_{l,z})}{|\mathbf{w}_b - \mathbf{u}_l|^2 \frac{du_{l,z}}{dx}} \quad (12)$$

where  $\mathbf{u}_l$  is the velocity of the liquid.

### SIMULATION SETTINGS

All the simulations for the air-water system were carried out on an 80x80x80 grid with the bubble positioned at 2/3 height in the centre of the box. For the toluene-water system an Eulerian grid of 80x80x200 cells was used with the bubble positioned at 70% height of the box. In both cases the initially spherical bubble was 20 Eulerian cells in diameter.

A moving window concept was used for all the simulations to ensure that no computational power is wasted and the bubble is always at the same distance from the walls. Finally, free-slip boundaries are used for all the walls.

Absence of grid dependency was verified by running simulations at a lower resolution. The same values were found for the steady rise velocities.

With the improvements in the numerical implementation of the FT model, it was possible to simulate very small bubbles (~1 mm diameter) with realistic properties

without numerical instabilities or numerically caused changes in volume of the disperse elements.

The physical properties of the air, water and toluene used are given in Table 1. They are taken at a standard temperature of 25 °C and a pressure of 1.0 bar.

Phase	Viscosity [kg·m <sup>-1</sup> ·s <sup>-1</sup> ]	Density [kg·m <sup>-3</sup> ]	Surface tension [N·m <sup>-1</sup> ]
Water	1.0·10 <sup>-3</sup>	1000	0.073
Toluene	5.9·10 <sup>-4</sup>	860	-
Air	1.8·10 <sup>-5</sup>	1.25	-

**Table 1:** Physical properties of the different materials used in the simulations.

### DRAG FORCE

First the simulation results for the drag force for the air-water system will be discussed. Subsequently, the results for toluene droplets in water will be presented.

#### Air bubbles in water

Each bubble in the simulations is initially spherical and the fluid is at rest. Therefore initially the bubble velocities for bubbles of different diameter will be the same. After some time the bubbles take their final shape and they reach their terminal rise velocity (Fig. 3). It can be seen that the 3, 4 and 5 mm bubbles exhibit a sinusoidal oscillation, of which the amplitude increases with the bubble size. Simulations for larger bubbles have been successfully completed, but the wobbling motion of the bubbles becomes highly irregular. In reality these bubbles probably break-up. Break-up of bubbles has not been implemented in the FT model and therefore the results are not included in the graph.

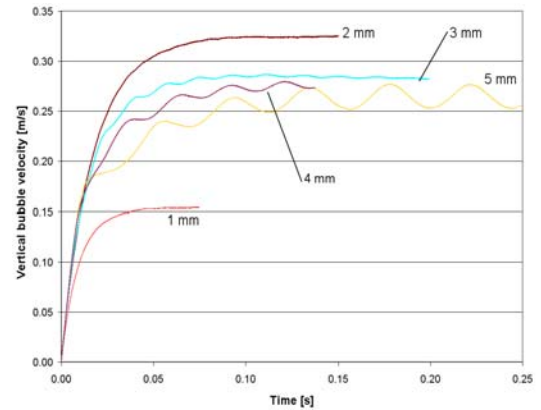


**Figure 3:** Simulated rise velocity as a function of time for air bubbles in pure water.

A big advantage of FT is the highly detailed information on the bubble interface, which can directly be visualised (Fig. 4). It can be seen that small (~ 1 mm) bubbles are almost spherical, while the larger bubbles become increasingly more deformed. The largest two bubbles keep alternating their shape.

Finally, the drag coefficient can be computed from the terminal rise velocity of the bubbles. This makes it possible to compare different correlations for the drag force in dimensionless units (Fig. 5). It can be seen that there is some discrepancy between the different

experimental relations, especially for small bubbles (1-2 mm). Overall, the simulations agree reasonably well with the experimental correlations.

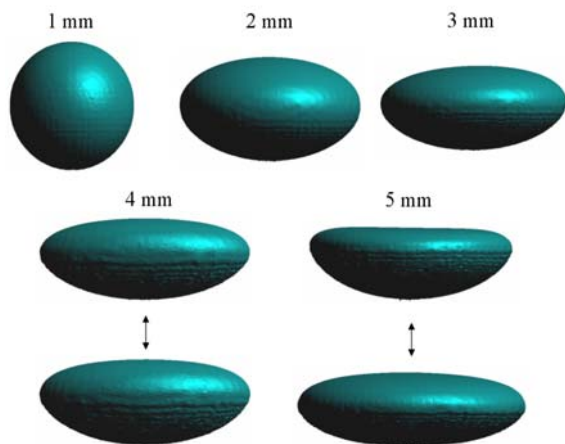


**Figure 4:** Bubble interface for different air bubbles rising in water, calculated by the FT model.

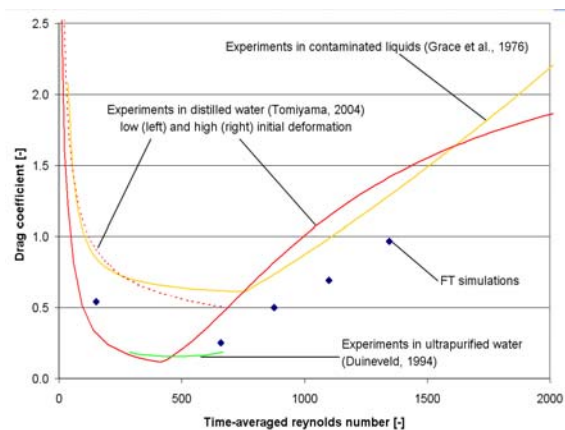


**Figure 5:** Drag force coefficient as a function of the Reynolds number for both experiments from literature and FT simulations performed in this work.

The famous relation by Grace et al. (1976) for contaminated liquids is included in Fig. 5, because its use has become widespread over the years. There is also a correlation available for pure water systems, but it is very unreliable due to the large scatter in the experimental data.

Tomiya (1998) derived a drag law for a wide range of fluid properties, which is a combination of existing empirical relations and relations derived from a force balance for a bubble in an infinite liquid. This model was validated on basis of a large number of measurements for air bubbles in distilled water (Tomiya, 2004). He found that the initial shape deformation during injection influences the terminal rise velocity of the bubble and therefore his measurements are scattered over the whole area surrounded by the indicated lines. This effect was separately confirmed by Wu and Gharib (2002).

The measurements by Duineveld (1994) were performed in “hyper clean” water, with a very gentle injection method. Note that in the simulations contaminants are not accounted for and the bubble is released in the most subtle way possible, which makes these data the best comparison. It can be seen that at a Reynolds number

above 450 the bubbles in hyper clean water (Duineveld) experience less drag than those in distilled water (Tomiya). The FT result for a 2 mm air bubble agrees very well with the experimental results by Duineveld. Unfortunately Duineveld only measured bubbles with a diameter in the range of 0.7 to 2.0 mm. Therefore future work will focus on simulating bubbles in the interesting region between 1 and 2 mm.

#### Toluene droplets in water

The same types of simulations have been carried out for toluene droplets in water. It is interesting to compare these systems, because the Morton number is almost the same ( $2.9 \cdot 10^{-11}$  for toluene in water versus  $2.5 \cdot 10^{-11}$  for air in water). However, due to the denser dispersed phase, its inertia will be much higher which affects the bubble motion.

First of all the rise velocity is given in Figure 6 for toluene droplets with an equivalent sphere diameter of 4–12.5 mm. It can be seen that all the droplets have more or less the same velocity equal to 0.14 m/s, which is typical behaviour for the inertia dominant regime. Droplets larger than 5 mm oscillate in a sinusoidal manner, with higher amplitudes for larger droplets.

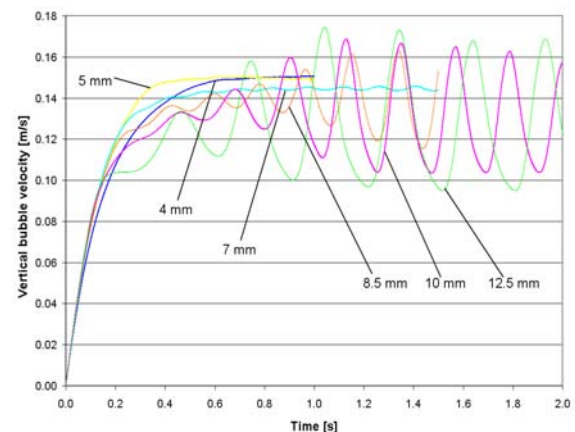


**Figure 6:** Simulated rise velocity as a function of time for toluene droplets in pure water.

In Fig. 7 the shape for differently sized droplets is visualized. The changes in interface shapes for the wobbling droplets are more pronounced than those of air bubbles in water, which can be attributed to the much larger mass of the droplet.

Finally the drag force coefficient is plotted as a function of Reynolds number (Fig. 8). It can be seen that the FT simulation results correspond reasonably well with the experimentally obtained relation by Tomiyama (2004) for pure bubbles. Note that this relation was analytically derived (Tomiya, 2002) and is not only valid for air/water systems.

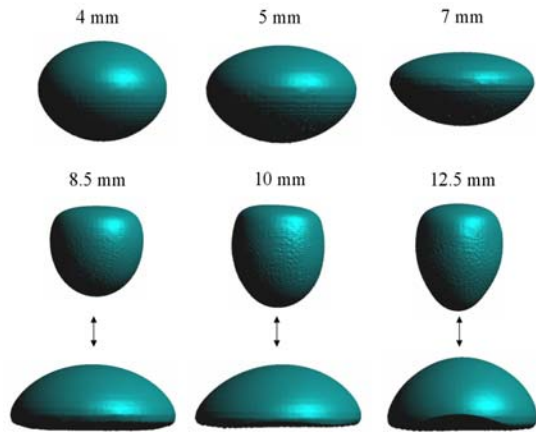


**Figure 7:** Bubble interface for different toluene droplets rising in water, calculated by the FT model.

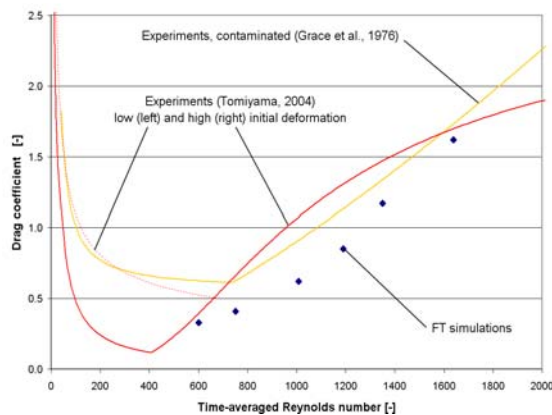


**Figure 8:** Drag force coefficients for toluene droplets in water, as a function of the Reynolds number.

### VIRTUAL MASS FORCE

The virtual mass coefficient for a spherical object can be calculated from potential flow theory and is equal to 0.5. It has been shown by Mouguin and Magnaudet (2002) that this value may also be used for a spherical bubble in a viscous flow. For a gas bubble this means that the bubble will accelerate with almost twice the gravitational acceleration.

From the same simulations as for the drag force a value of 0.53 was found for all the different air bubbles, which agrees well with theory, considering that the bubble is only 20 grid cells in diameter. A detailed analysis of the grid-dependency shows that this value indeed converges to the analytical value of 0.50.

### LIFT FORCE

In order to complete the closures for a discrete element model the lift force has to be studied. Because of the wobbling motion of the dispersed elements the simulations must be run for a few seconds, which takes several months real time on a single CPU. Therefore until now only 0.5 seconds have been simulated for a 4 mm air bubble in water with a linear shear of  $5 \text{ s}^{-1}$ . Figure 9 shows the shape of the bubble during one oscillation cycle. Note that the image has not been postprocessed in any way and this is exactly how the interface is accounted for in the simulation. It can be seen that the shape is very dynamic,

but the FT model is still able to describe it with great detail.

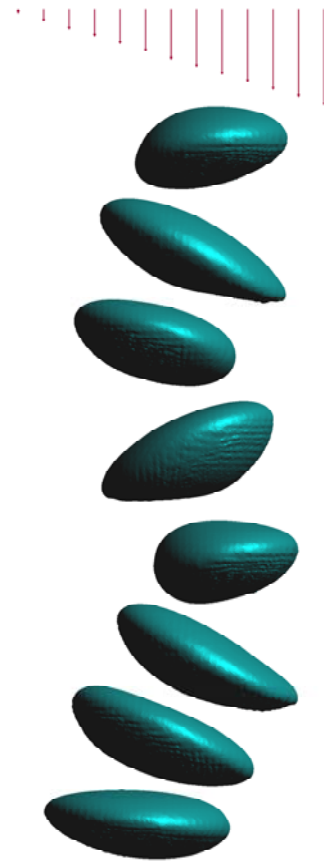


**Figure 9:** The bubble interface at different times during one oscillation cycle of a 4 mm air bubble in water with a shear rate of  $5 \text{ s}^{-1}$ .

The position of the bubble as a function of time is given in Figure 10. Initially the bubble is spherical and during the first 0.25 seconds it deforms until it comes to a more-or-less stationary oscillatory motion. After this the bubble has attained a net movement towards the side with the highest velocity (positive horizontal direction).

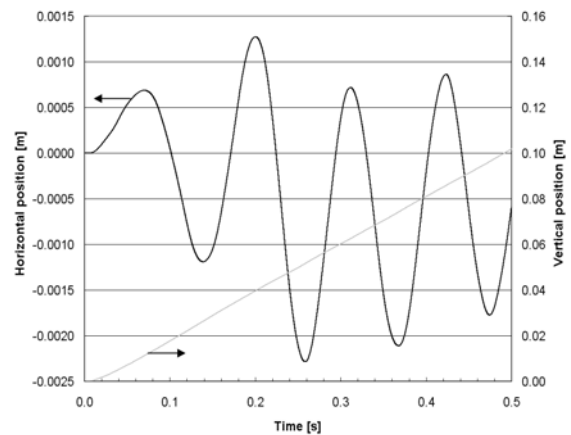


**Figure 10:** Bubble trajectory during the first 0.5 seconds of the simulation for a 4 mm air bubble in a linear shear field.

A time-averaged lift coefficient of 0.5 was found, which is higher than the value of 0.3 measured by Tomiyama et al. (2002b). It should be noted however that his measurements were performed at low Reynolds numbers ( $< 50$ ), while in the simulation a Reynolds number in the order of 1000 is reached. This explains why the experimental bubbles are rising more or less along a straight line, while air bubbles in water are meandering from left to right. More work needs to be carried out using different shear rates and bubble diameters for longer simulation times.

## CONCLUSIONS

A 3D FT model was developed and used to investigate closures for the interface forces acting on dispersed elements, viz. air bubbles and toluene droplets, in water. The improvements of the numerical implementation of the FT model allowed the simulation of very small air bubbles ( $\sim 1$  mm) in water using realistic physical properties without numerical instabilities or significant numerically caused volume changes of the air bubble. According to the authors' knowledge this is the first time that simulation results for such small air bubbles in water using realistic physical properties are reported.

The computed drag coefficients for air bubbles in water with a diameter ranging from 1-5 mm compare well with experimentally obtained results for ultra pure water. Similar drag coefficients were computed for toluene droplets in water, as expected for systems with comparable Morton numbers.

A virtual mass force coefficient of 0.53 has been found for air bubbles in water with an equivalent diameter of 1-5 mm using an  $80 \times 80 \times 80$  grid. With a higher grid resolution the value indeed converged to the expected theoretical value of 0.50.

For a 4 mm air bubble in water a lift force coefficient of 0.5 was found, which is somewhat higher than was reported in the literature at lower Reynolds numbers. In the future the lift force coefficient will be studied for different bubble sizes, shear rates and longer simulation times.

## ACKNOWLEDGEMENT

This work is part of the research programme of the Stichting voor Fundamenteel Onderzoek der Materie (FOM), financially supported by the Nederlandse Organisatie voor Wetenschappelijk Onderzoek (NWO) and Shell Global Solutions.

## REFERENCES

CENTRELLA, J. and WILSON, J., (1984), "Planar Numerical Cosmology, II, The difference equations and numerical tests", *Astrophysical J. Supplement Series*, **54**, 229-249.

DEEN, N.G., VAN SINT ANNALAND, M. and KUIPERS, J.A.M., (2004), "Multi-scale Modeling of Dispersed Gas-Liquid Two-Phase Flow", *Chem. Eng. Sci.*, **59**, 1853-1861.

DUINEVELD, P.C., (1994), "Bouncing and coalescence of two bubbles in water", Ph.D. thesis, University of Twente, The Netherlands.

GRACE, J.R., WAIREGI, T. and NGUYEN, T.H., (1976), "Shapes and velocities of single drops and bubbles moving freely through immiscible liquids", *Trans. Instn. Chem. Engrs.*, **54**, 116-120.

GUNSING, M., (2004), "Modelling of bubbly flows using volume of fluid, front tracking and discrete bubble models", Ph.D. thesis, University of Twente, The Netherlands.

LAMB, H., (1932), "Hydrodynamics", Cambridge University Press, London.

MOUGUIN, G. and MAGNAUDET, J., (2002), "The generalized Kirchhoff equations and their application to the interaction between a rigid body and an arbitrary time-dependant viscous flow", *Int. J. Multiphase Flow*, **28**, 1837-1851.

POPINET, S. and ZALESKI, S., (1999), "A Front Tracking algorithm for the accurate representation of surface tension", *Int. J. Numer. Methods Fluids*, **30**, 775-794.

PROSPERETTI, A., (2001), "Navier-Stokes numerical algorithms for free-surface flow computations: An overview", *Drop Surface Interactions*, **21**.

SCARDOVELLI, R. and ZALESKI, S., (1999), "Direct Numerical Simulation of Free Surface and Interfacial Flow", *Annu. Rev. Fluid Mech.*, **31**, 567-603.

TOMIYAMA, A., (1998), "Struggle with Computational Bubble Dynamics", *Third Int. Conf. on Multiphase Flow*, Lyon, France.

TOMIYAMA, A., CELATA, G.P., HOSOKAWA, S. and YOSHIDA, S., (2002a), "Terminal velocity of single bubbles in surface tension force dominant regime", *Int. Journal Of Multiphase Flow*, **28**, 1497-1519.

TOMIYAMA, A., TAMAI, H., ZUN, I. and HOSOKAWA, S., (2002b), "Transverse migration of single bubbles in simple shear flows", *Chemical Engineering Science*, **57**, 1849-1858.

TOMIYAMA, A., (2004), "Drag, lift and virtual mass forces acting on a single bubble", *3<sup>rd</sup> Int. Symp. On Two-Phase Modeling and Experimentation*, Pisa, Italy, September 22-24.

TRYGGVASON, G., BUNNER, B., ESMAEELI, A., JURIC, D., AL-RAWAHI, N., TAUBER, W., HAN, J., NAS, S. and JAN, Y.J., (2001), "A front tracking method for the computations of multiphase flow", *J. Comp. Phys.*, **169**, 708-759.

UNVERDI, S.O. and TRYGGVASON, G., (1992), "A front-tracking method for viscous incompressible multi-fluid flows", *J. Comp. Phys.*, **100**, 25-37.

VAN SINT ANNALAND, M., DEEN, N.G. and KUIPERS, J.A.M., (2003), "Multi-Level Modelling of Dispersed Gas-Liquid Two-Phase Flows. Series: Heat and Mass Transfer. Editors: M. Sommerfeld and D. Mewes", Springer-Verlag, 139-157.

VAN SINT ANNALAND, M., DEEN, N.G. and KUIPERS, J.A.M., (2005a), "Numerical simulation of gas bubbles behaviour using a three-dimensional Volume of Fluid method", accepted for publication, *Chem. Eng. Sci.*

VAN SINT ANNALAND, M., DIJKHUIZEN, W., DEEN, N.G. and KUIPERS, J.A.M., (2005b), "Numerical simulation of gas bubbles behaviour using a three-dimensional Front Tracking method", submitted, *AIChe J.*

WU, M. and GHARIB, M., (2002), "Experimental studies on the shape and path of small air bubbles rising in clean water", *Phys. Fluids*, **14**, L49-52.